Self-Assembly Hot Paper

How to cite: *Angew. Chem. Int. Ed.* **2022,** *61,* e202200390
International Edition: doi.org/10.1002/anie.202200390
German Edition: doi.org/10.1002/ange.202200390

Anti-cooperative Self-Assembly with Maintained Emission Regulated by Conformational and Steric Effects

Ingo Helmers[+], Muhammad Saddam Hossain[+], Nils Bäumer, Paul Wesarg, Bartolome Soberats, Linda S. Shimizu, and Gustavo Fernández**

Abstract: Herein, we present a strategy to enable a maintained emissive behavior in the self-assembled state by enforcing an anti-cooperative self-assembly involving weak intermolecular dye interactions. To achieve this goal, we designed a conformationally flexible monomer unit **1** with a central 1,3-substituted (diphenyl)urea hydrogen bonding synthon that is tethered to two BODIPY dyes featuring sterically bulky trialkoxybenzene substituents at the *meso*-position. The competition between attractive forces (H-bonding and aromatic interactions) and destabilizing effects (steric and competing conformational effects) limits the assembly, halting the supramolecular growth at the stage of small oligomers. Given the presence of weak dye–dye interactions, the emission properties of molecularly dissolved **1** are negligibly affected upon aggregation. Our findings contribute to broadening the scope of emissive supramolecular assemblies and controlled supramolecular polymerization.

Introduction

Supramolecular polymers have become privileged materials due to their unique properties resulting from their dynamic and reversible self-assembly, such as self-healing or stimuli-responsiveness.[1] Their exciting photophysical properties make them prime candidates for the design of functional materials in various fields, including optoelectronics and biomedicine.[2,3] Nevertheless, a major challenge in supramolecular polymerization lies in the difficulty of finely controlling molecular interactions during the assembly process. Given that the vast majority of supramolecular polymers are based on π-conjugated building blocks,[4,5] the lack of controlled self-assembly typically results in unpredictable photophysical properties. In many cases, the highly preorganized, generally steric-free aromatic surface of most chromophores favors strong face-to-face dye interactions rendering non-emissive H-type aggregates (Scheme 1).[6,7] This limitation can be commonly overcome in two different ways: i) introducing sterically bulky substituents in the molecular design, typically at the chromophore's core,[8,9–11] or ii) including chromophores with various freely-rotating

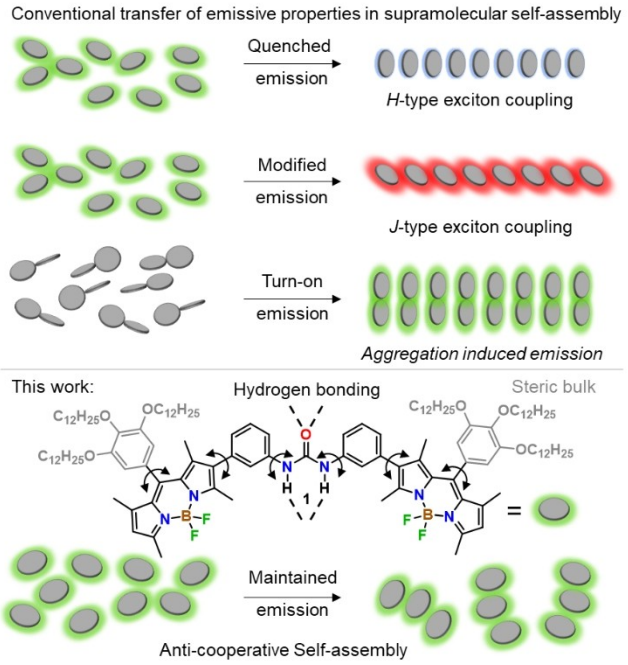

Scheme 1. Top: Summary of different types of transfer of emissive properties in supramolecular self-assembly. Bottom: Molecular structure of urea-based BODIPY **1** and cartoon representation of its anti-cooperative self-assembly into discrete species with maintained emission.

[*] Dr. I. Helmers,[+] N. Bäumer, P. Wesarg, Prof. Dr. G. Fernández
Organisch-Chemisches Institut
Westfälische Wilhelms-Universität Münster
Corrensstraße 36, 48149, Münster (Germany)
E-mail: fernandg@uni-muenster.de

M. S. Hossain,[+] Prof. Dr. L. S. Shimizu
Department of Chemistry and Biochemistry
University of South Carolina
Columbia, SC 29208 (USA)
E-mail: shimizls@mailbox.sc.edu

Dr. B. Soberats
Department of Chemistry
University of the Balearic Islands
Cra. Valldemossa, Km. 7.5, 07122 Palma de Mallorca (Spain)

[+] These authors contributed equally to this work.

groups that undergo restriction in intramolecular rotation (RIR) upon aggregation (Scheme 1).[12,13] While the former strategy often induces a J-type aggregation process with red-shifted absorption and emission,[11,14,15] the latter approach leads to a turn-on or a dramatic amplification of the emission compared to the monomer species *via* aggregation-induced emission (AIE).[12,16] Thus, self-assembly of π-conjugated building blocks generally results in significant changes in the original photophysical properties of the system.

The difficulty in preserving emissive properties upon self-assembly can be understood considering commonly employed monomer design approaches. Typically, aromatic interactions between dye molecules are exploited in order to favor aggregation in various solvent systems.[4,17] This approach is indeed effective to drive a one-dimensional growth; it, however, often fails to create aggregates with a high degree of internal order.[3,18,19]

To overcome this limitation, functional groups that can engage in directional non-covalent forces, such as hydrogen bonding, are included in the molecular design. This widely used strategy proves successful to increase the stability and degree of order of the resulting supramolecular polymers, generally leading to highly elongated one-dimensional cooperatively formed assemblies.[20] However, this comes at the cost of strong dye–dye interactions, which inevitably leads to significant changes in the photophysical behavior. Accordingly, new alternatives to control the extent of exciton coupling of monomer units will allow for a more readily available knowledge transfer between photophysical properties in the molecular and the self-assembled state.

To achieve this goal, we hypothesize that strategies to limit self-assembly, including incorporation of anti-cooperative effects, would enable control of the assembly size[21] and allow fine-tuning of chromophore organization. Unlike the widely oberved isodesmic and cooperative mechanisms, examples of anti-cooperative self-assembly remain scarce,[22–26] and drawing up general design rules to attenuate the growth of supramolecular polymers into discrete sizes is challenging.[27] While a careful balance of solvent polarity, temperature, concentration or end-capping can lead to a certain level of size limitation, a hard coded size control can be difficult to achieve.[28] Typical molecular design strategies rely on the use of hydrogen bonding,[24,29] or dipole moment cancellation[22,30] to favor particularly stable dimer conformations after which elongation is disfavored. On the other side, in some cases, the weakening of the elongation step by steric[25,26,31–34] or coulombic[35] repulsive interactions may also favor an attenuated anti-cooperative growth.

Herein, we exploit self-limiting growth strategies that combine conformational and steric effects to regulate inter-chromophore interactions in self-assembly, leading to anti-cooperatively formed oligomeric assemblies with maintained emission. For this purpose, we selected a conformationally flexible monomer unit with a central 1,3-substituted (diphenyl)urea hydrogen bonding synthon that is tethered to two BODIPY dyes featuring sterically bulky trialkoxybenzene substituents at the *meso*-position (see compound **1** in Scheme 1; for synthesis and characterization, see the Supporting Information). This molecular design enables an appropriate balance of attractive forces (hydrogen bonding and aromatic interactions) and destabilizing effects (steric effects and multiple possible monomer conformations due to a high conformational freedom) that are required to suppress an elongated growth.[9–11,15] As a result, we were able to increase the dye-dye distances, thereby attenuating the aggregation at the stage of short oligomers and leading to maintained emission compared to the monomer state. This new strategy broadens the scope of anti-cooperative self-assembly and might facilitate an adequate transfer of photophysical properties from the molecular to the self-assembled state.

Results and Discussion

Mechanistic Insights into the Self-Assembly of 1

Initial self-assembly studies of **1** were conducted using UV/Vis spectroscopy. In a range of polar organic solvents at $c =$ 10 and 100 μM, typical absorption spectra of monomeric BODIPY are obtained for **1** at room temperature (RT): a sharp $S_0 \rightarrow S_1$ transition centered at around 518 nm and a less intense $S_0 \rightarrow S_2$ transition band at 377 nm (Figure 1a (red spectrum) and S7). On the other hand, a slight decrease of absorbance along with a minor red shift of the absorption maximum ($\lambda_{max} = 520$ nm, $\Delta\lambda = 2$ nm) are observed in non-polar methylcyclohexane (MCH) (blue spectrum in Figure 1a, see also Figure S7). Additionally, a broadening of the main absorption band is observed, suggesting the formation of an aggregated species (**Agg1**) in MCH. This atypical aggregate absorption spectrum, almost unaltered in comparison to the monomer, suggests the presence of weak aromatic interactions between the BODIPY dyes.[11,15]

Complementary emission studies ($\lambda_{exc} = 500$ nm, Figure 1b) disclose a single, intense emission band for both monomer ($\lambda_{max} \approx 541$ nm) and aggregate (**Agg1**, $\lambda_{max} \approx 549$ nm), which supports the hypothesis of weak exciton coupling of the dyes in the aggregated state. Interestingly, as a result of this effect, a remarkable quantum yield (φ_F) is obtained upon aggregation in MCH, almost as high as that determined for the monomer in $CHCl_3$ (see emission intensity of the monomer and aggregate solutions, inset Figure 1b, **1** (mon): $\varphi_F = 30\,\%$ and **Agg1**: $\varphi_F = 26\,\%$). Even though the φ_F values are within a similar range of other BODIPY dyes reported in the literature,[36–38] the nearly unchanged φ_F in non-polar solvents upon aggregation is a highly unusual observation.[36,37] Typically, strong H-type exciton coupling leads to a drastic reduction of fluorescence quantum yields,[36] while J-Aggregates can lead to a slight decrease,[37] as well as increase in fluorescence quantum yield,[38] depending on the accessibility of nonradiative pathways.[39] These results highlight the efficient retention of emissive properties based on molecular design. Additionally, time resolved photoluminescence decay studies found a similar average lifetime for both species, which confirms the weak influence of the aggregation on the emissive properties (Figure S8, Table S8).

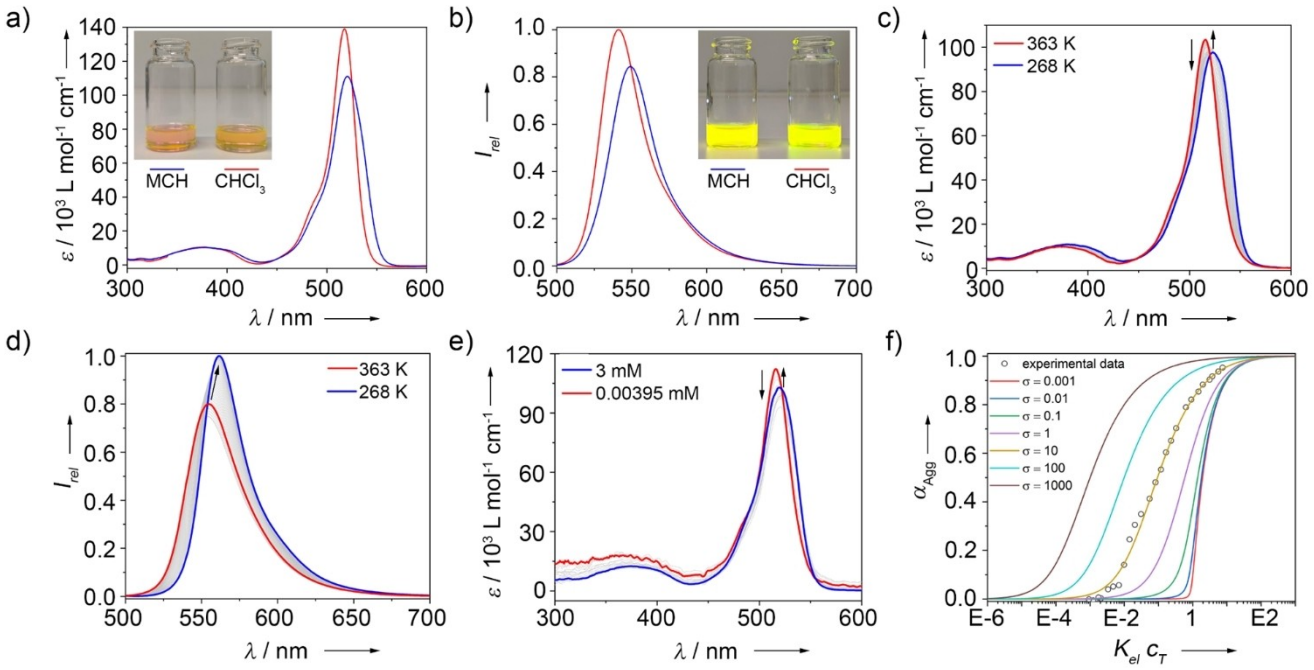

Figure 1. Absorption (a) and emission spectra (b, $\lambda_{exc}=500$ nm) of compound **1** in a molecularly dissolved ($CHCl_3$, inset: right solution) and aggregated state (MCH, inset: left solution) ($c=10$ mM, $T=298$ K). VT-Absorption (c) and VT-emission spectra (d, $\lambda_{exc}=500$ nm) in MCH ($c=20$ μM, 10 K min^{-1}, 363 K–268 K). e) Concentration-dependent absorption studies in MCH at 333 K. f) Goldstein–Stryer fit with variable σ at 333 K.

Besides the weak dye coupling, another plausible explanation for the high emission intensity in MCH might be the formation of J-type aggregates. However, this hypothesis can be ruled out, as the red-shift in absorption ($\Delta\lambda=2$ nm) is insignificant and the Stokes shift is higher with respect to the monomer ($\Delta\tilde{\nu}_{mon}=821$ cm^{-1} vs. $\Delta\tilde{\nu}_{agg}=1016$ cm^{-1}, Figure S7), which are not in agreement with a typical J-type aggregation process.[7,40]

The reversibility of the monomer-to-aggregate transformation was next investigated in MCH using variable temperature (VT) emission and absorption spectroscopy covering a broad concentration range (0.4 μM–3 mM; Figures 1c,d and S9–S18). Upon cooling monomer solutions of **1** in MCH from 363 K to 268 K, a small red-shift of the maximum and a broadening of the main absorption band are observed (Figure 1c). The spectral changes are independent of the cooling ramp (0.1 K min^{-1} vs. 10 K min^{-1}), which highlights the thermodynamic stability of **Agg1** (Figure S8).[19,41] Intriguingly, VT-emission studies in MCH show slightly higher emission intensity for **Agg1** at low temperatures compared to the monomer state at high temperatures (Figure 1d). These findings underline that the emission properties of the monomer state are preserved upon self-assembly. Thermodynamic insights into the underlying self-assembly mechanism of **1** were obtained by monitoring the absorption changes at 530 nm for 25 different concentrations (0.4 μM–3 mM) and subsequent fitting to the isodesmic model[42] (Figures S10–S18, Table S1). However, at this stage, the experimental data points deviate from a perfect sigmoidal curve, which suggests that an anti-cooperative mechanism may be operative.[24–26,29]

In order to further inspect the self-assembly mechanism of **1**, we performed additional concentration-dependent absorption studies at constant temperatures in a range between 273 K and 363 K. In agreement with VT-studies, monitoring the spectral changes against concentration reveals sigmoidal-like curves lacking a critical concentration with a sudden onset of self-assembly, which rules out a conventional cooperative assembly process. Thus, the obtained plots can only be explained considering either an isodesmic or an anti-cooperative mechanism. In order to address this matter, we analyzed the extracted data with a weakly anti-cooperative ($\sigma=10$) vs. isodesmic fit ($\sigma=1$) using the Goldstein–Stryer model (Figures 1f and S19–S22).[43] Especially in the lower ($\alpha_{agg}=0.0$–0.1) and upper ($\alpha_{agg}=0.9$–1.0) aggregation regimes, discrepancies to an isodesmic process are found and the experimental data points are more accurately described by a weakly anti-cooperative model (Figure S19–S22). The derived thermodynamic parameters (van't Hoff plot, Figure S22) using the isodesmic and the anti-cooperative nucleation process (energetically most favorable state) only exhibit minor differences. However, the elongation process is discarded in the isodesmic fit and the thermodynamic parameters of this process exhibit a higher discrepancy in the standard entropy and, consequently, in the free Gibbs energy (Figures S19–S22, Table S2–4). Likely, the dominance of strong steric repulsion upon aggregate growth frustrates the supramolecular polymerization, halting the growth at the stage of small oligomeric structures for **1**. This would be a reasonable explanation for the small absorption and emis-

sion changes observed for **1**, even at high (mM) concentrations.

Conformational analysis of 1

In order to rationalize the origin of the experimentally observed weak anti-cooperative self-assembly process, the various molecular elements of **1** need to be considered. In addition to a urea hydrogen bonding synthon, aromatic moieties and sterically bulky trialkoxybenzene groups, **1** has several rotatable single bonds that provide the system with some conformational freedom. As a result, competing monomer conformations may strongly influence the (pre)nucleation of **1**, thereby determining the self-assembly outcome.[44] Due to the unsymmetrical *meta*-substitution pattern of the benzene rings connecting the BODIPYs and the urea motif, three distinct conformations are possible: *syn–syn*, *syn–anti* and *anti–anti* (Figure 2d). A computational approach was utilized to investigate this complex monomer energy landscape using TD-DFT in the gas phase (ωB97X-D[45]/6-31G*[46]). The dodecyloxy side chains were reduced to methoxy to decrease computational expenses. ωB97X-D is a long-range corrected hybrid density functional with dispersion correction that is particularly suited for BODIPY derivatives.[47] Further computational details are given in the Supporting Information. In accordance with the literature, the calculations predict that the urea group of **1** prefers the *trans–trans* conformation.[48] With regards to the relative orientation of the BODIPY units, the three previously mentioned conformers (*syn–syn*, *syn–anti* and *anti–anti*) were optimized (Figure 2d). According to the calculations, the following conformer stability is predicted from more to less stable: *syn–anti* > *anti–anti* ($+5\ kJ\,mol^{-1}$) > *syn–syn* ($+7\ kJ\,mol^{-1}$) (Figure 2d, Table S10). The highest stability of the *syn–anti* conformation can be rationalized by the opposite orientation of the BODIPY dyes on both sides of the urea, which minimizes potential steric effects. On the other hand, in the *anti–anti* conformation, the two BODIPY cores are oriented oppositely to the urea carbonyl forming a ca. 90° angle (Figure 2d). The closer distances between the BODIPY cores in this conformation accounts for its slightly lower stability compared to the *syn–anti* conformation. Finally, the energetically less stable *syn–syn* conformation is the one with the closest distance between the BODIPY centers (B···B) (16.8 Å for *syn–anti*, 15.0 Å for *anti–anti*, and 8.9 Å for *syn–syn*).

While our gas phase computations predict that the *syn–anti* conformation of monomer **1** is energetically more stable, crystal structures of simple 1,3-disubstituted phenyl ureas reveal that the *anti–anti* conformer is preferred in the solid state.[49] In the literature examples, the substituents were halogens or methyl, versus our BODIPY core. It is possible that the *anti–anti* conformation, even if less stable than the *syn–anti* form, may be the preferred conformation of **1** in the self-assembled state. Or more likely a complex

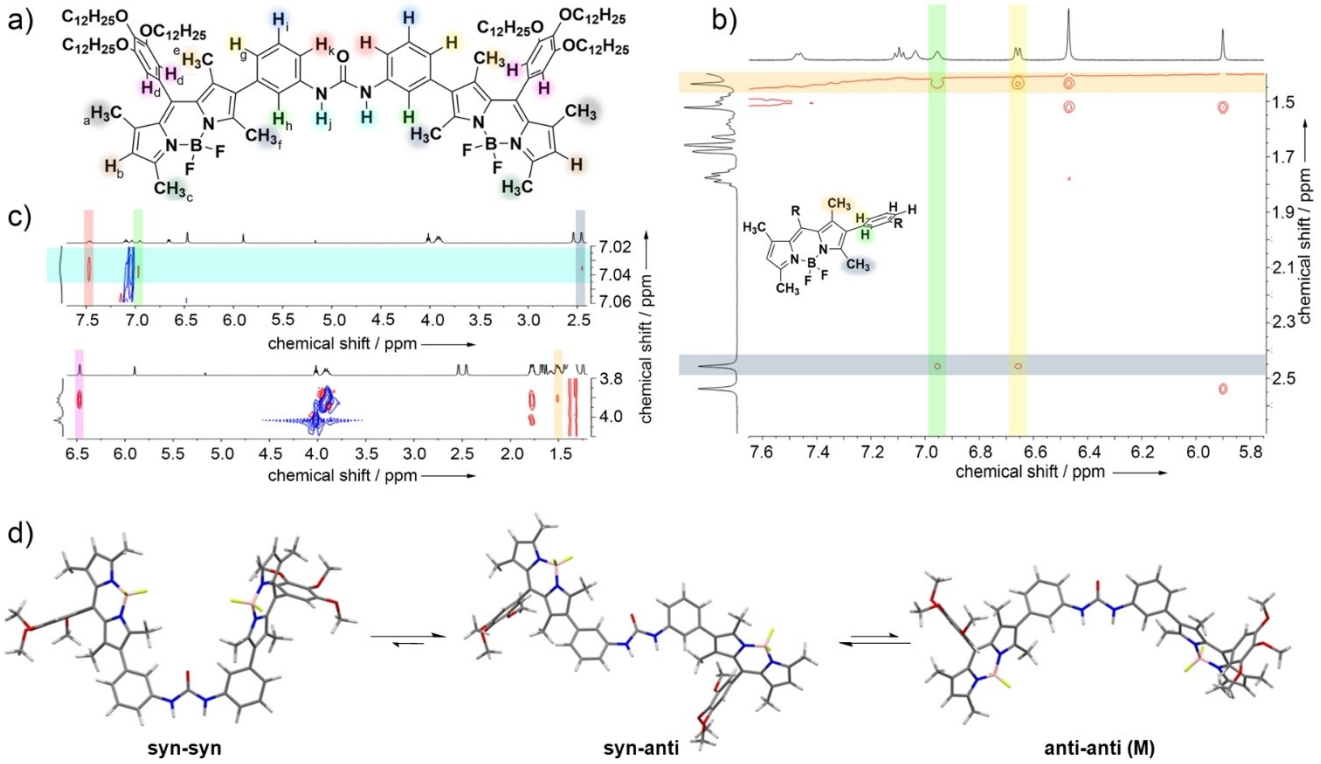

Figure 2. a) Molecular structure of **1**. b), c) 2D ROESY NMR experiments of **1** in $CDCl_3$ ($c = 10$ mM, 333 K). d) Optimized geometry and relative stability of BODIPY conformations using ωB97X-D/6-31G* method in the gas phase. The dodecyloxy chains have been reduced to methoxy to decrease computational costs.

equilibrium between rotamers may be feasible in the monomer state, with the *syn–anti* possibly being the most stable conformation, which reaffirms the high conformational freedom encoded in the molecular design of **1**.

To experimentally probe the existence of conformers, the molecularly dissolved species in $CDCl_3$ was investigated by 2D NMR (COSY and ROESY, Figures 2a–c and S23–S25). Interestingly, the BODIPY methyl protons adjacent to the benzene spacer (H_e (orange) and H_f (grey)) couple with both protons H_g (yellow) and H_h (green) from the benzene spacer (Figure 2b and S24). Given that the BODIPY core must necessarily arrange out-of-plane with respect to the adjacent benzene spacers to avoid steric repulsion, the observed coupling signals suggest the existence of a fast equilibration between various rotamers. Otherwise, if the BODIPY units were arranged in a fixed conformation, only a single correlation signal (for instance $CH_3(H_e)$ with H_g but not with H_h) would be observed. An additional observation is the coupling between the aromatic protons from the benzene spacer (H_h (green) and H_k (red)) and the urea N-H protons (H_j (cyan), Figure 2c and S25). These findings indicate that the urea and the adjacent benzene rings are not perfectly arranged in-plane, as suggested by theoretical studies (Figure S38). Further, a potential contribution of various rotamers might occur. Additionally, the urea N–H (H_j) couples with one of the methyl groups of the BODIPY ($CH_3(H_f)$), which is only possible if both protons are pointing in the same direction, i.e. arranged in the same plane. Furthermore, the protons of the dodecyl chains exhibit a discrete coupling with the protons of the trialkoxybenzene ring (H_d (pink)) and with one methyl group ($CH_3(H_e)$) of the BODIPY dye. These findings indicate that the solubilizing aliphatic chains partially surround the aromatic BODIPY dye, which may induce steric effects that frustrate the assembly. Overall, 2D NMR experiments suggest a monomer structure of **1** potentially involving multiple rotamers and a high degree of conformational freedom, which may possibly contribute to the attenuated growth exhibited for **Agg1** (see below).

Analysis of Preorganization and Prenucleation Events

We next studied how the mixture of conformers evolves upon decreasing the polarity of the solvent. To this end, we performed solvent-dependent denaturation studies at various concentrations using MCH and $CHCl_3$ as "poor" and "good" solvent, respectively. The studies reveal an intriguing multistep transition between monomeric and self-assembled state at high concentrations, with a distinct pre-nucleation regime (Figure S28, S29). This observation prompted us to inspect the conformational changes of **1** during the preorganization step in more detail. To this end, we selected suitable experimental conditions of solvent system and concentration ($MCH/CDCl_3$ 1:1 (v/v), 10 mM) and subsequently subjected monomeric **1** to VT-^{1}H NMR experiments between 328 K and 298 K. Notably, the proton signals of the N–H urea group (H_j, cyan) and those of its neighboring aromatic rings H_k (red), undergo marked shifts to higher ppm values upon cooling (Figure 3a). Considering that all other proton signals of **1** remain sharp and invariant with temperature, the observed behavior can be partially explained by intramolecular hydrogen bonding between the urea C=O group and the neighboring C–H aromatic protons (H_k), with potential contributions of solvent-solute interactions.[50] Such intramolecular C–H···O interactions are preferred over the typical bifurcated urea hydrogen bonding patterns in nitrophenyl ureas, where the electron withdrawing nitro groups likely increase the acidity of the aryl H.[51] The relatively large shifts of the urea proton signals (Hj) cannot be solely explained by the previously mentioned intramolecular preorganization event *via* C–H···O hydrogen bonding.

Thus, this process is most likely concomitant with the initial stages of an oligomerization event driven by N–H···O

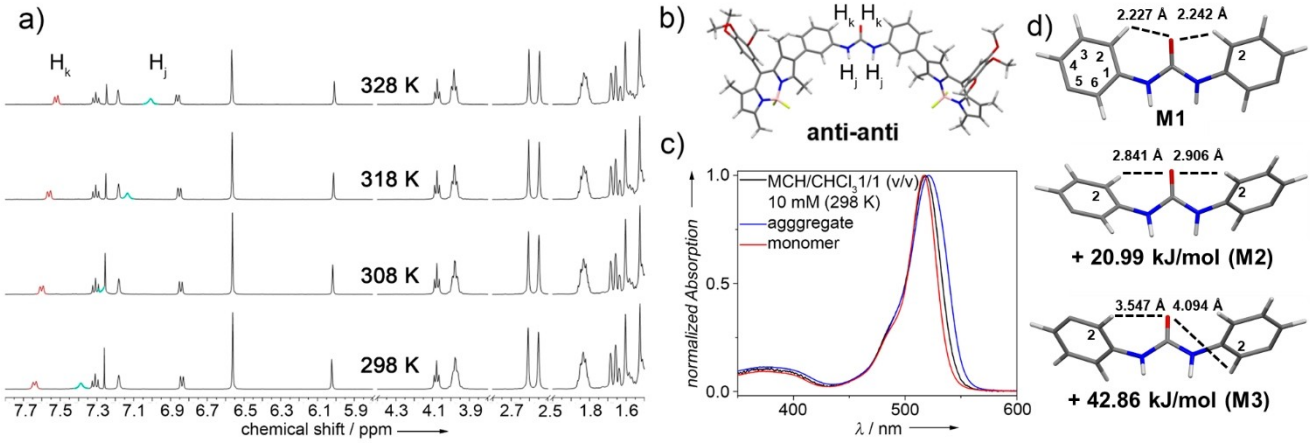

Figure 3. VT-^{1}H NMR (a) and absorption spectra (c) of **1** in MCH-d_{14}/$CDCl_3$ (1/1 (v/v), c = 10 mM cooling (5 K min^{-1}) from 328 K to 298 K. b) Optimized geometry of **1** *anti–anti* without geometric constraints using ωB97X-D/6-31G* method in the gas phase. d) Optimized structure using ωB97X-D/6-31G* method in the gas phase by freezing the linker urea and the attached benzene with variable intramolecular hydrogen bond length between CH(H_k)-CO(O).

hydrogen bonding, as also suggested by UV/Vis (see comparison of red and black spectra in Figure 3c). The potentially restricted intramolecular motion of **1** assisted by intramolecular C_{urea}=O···H_k–C(aromatic) interactions was further examined by TD-DFT. Three rotamers of the *anti-anti* conformer of **1** with different torsional angles between the urea carbonyl and the adjacent phenyl groups were optimized (**M1**: 15.66°, 18.27°; **M2**: 50.44°, 53.26°; **M3**: 74.76°, 80.40°) using a similar method (ωB97X-D/6-31G*, see Supporting Information for further computational details). Interestingly, the computations suggest that the overall stability of the structure dramatically decreases as the phenyl groups rotate out of the plane of urea, as seen in Figure 3d. The geometry of the *anti–anti* conformer and restricted rotation between CH(H_k)···CO(O) further supports the initial 2D NMR and VT-^{1}H NMR experiments. The same study was carried out with two additional functionals (B3LYP/6-31G*, and B3LYP-D3/6-31G*), yielding similar results (Table S11). We hypothesize that the intramolecular interaction C_{urea}=O···H_k–C(aromatic) restricts the molecular rotation of **1**, thereby preorganizing the monomer and making it more susceptible to further nucleation and oligomerization.

Interplay between Preorganization and Oligomerization

To investigate the interplay between intra- and intermolecular interactions in the self-assembly of **1**, we employed combined VT-^{1}H NMR, UV/Vis and FTIR experiments in pure MCH (c = 0.5 and 1 mM, 363 K–283 K). Given that solvophobic and aromatic interactions are favored under these conditions, **1** can reach a fully self-assembled state at low temperatures (283 K) (Figure 4 and S26, S27). On the other hand, at the highest temperature (363 K), a partially disassembled state (α_{agg} = 0.68) is achieved, as suggested by UV/Vis measurements at 1 mM (Figures 4c and S26). ^{1}H NMR studies at high temperatures (363 K) reveal relatively sharp signals (Figure 4a), highlighting the existence of weak intermolecular interactions of the chromophores of **1** under these conditions. This is supported by the presence of a single carbonyl stretching band at 1724 cm^{-1} in FTIR (Figure 4b). Interestingly, controlled cooling from 363 K to 283 K allows the identification of the previously mentioned pre-organization and oligomerization steps, the latter becoming more prominent at lower temperatures. At intermediate temperatures (323 K), the deshielding of the proton signals H_k is in accordance with the preorganization step *via* intramolecular C_{urea}=O···H_k–C interactions (Figure 4a–c). As a result of this rotational restriction, aromatic interactions become feasible in this low-polarity medium (MCH), as

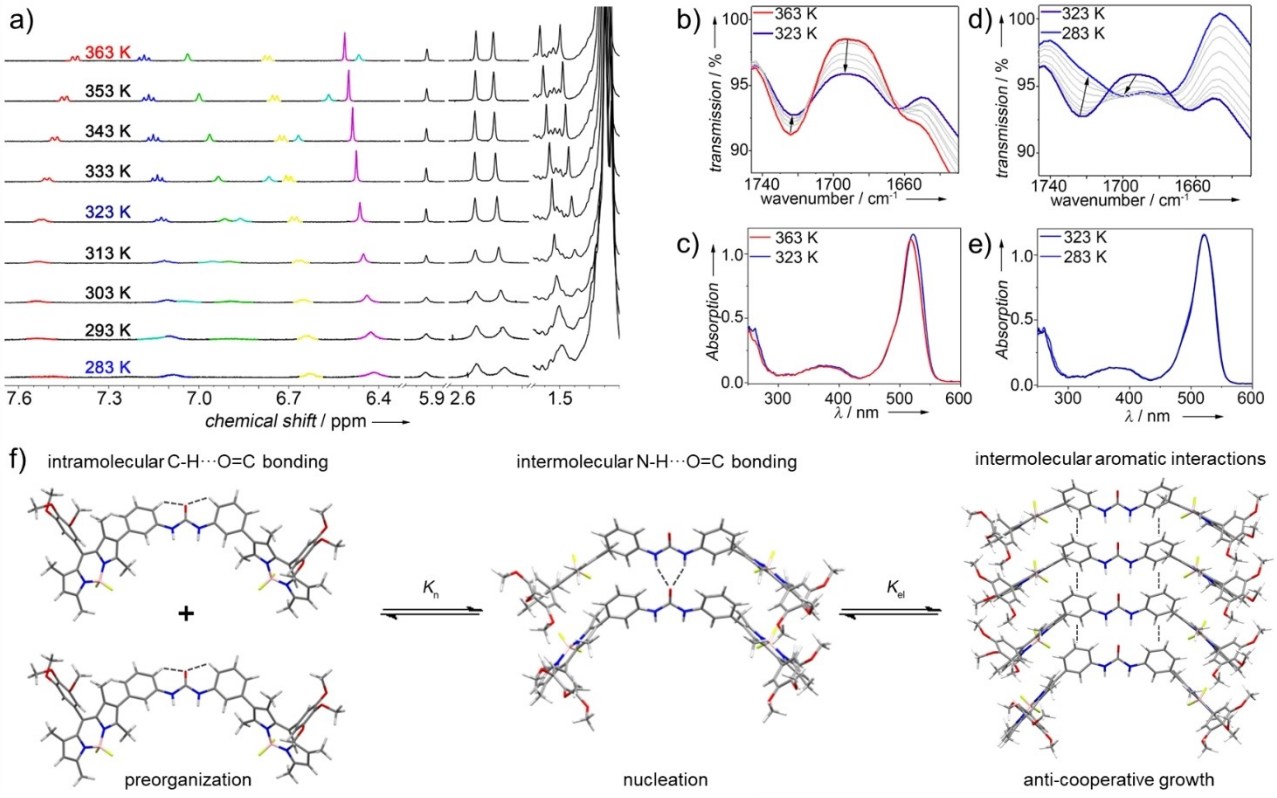

Figure 4. VT-^{1}H NMR (a), FT-IR (b, d) and absorption spectra (c, e) of **1** in MCH-d_{14}/$CDCl_3$ (1 : 1; v/v, c = 1 mM, a) and in MCH (c = 1 mM, b–e) cooling from 363 K to 283 K, using a cooling rate of 5 K min^{-1} (a, c and e). f) Optimized monomer, dimer and tetramer structures of **1** highlighting the different steps in the self-assembly process (calculations were perfomed using the ωB97X-D/6-31G* method (monomer) or the semi-empirical PM6 method (dimer and tetramer) respectively).

indicated by the concomitant shielding of the proton signals of the benzene spacers adjacent to the urea group ($H_{g\text{-}i}$). In sharp contrast, the BODIPY methyl groups exhibit almost no shifts and no broadening upon cooling (Figure 4a, black resonances) in this temperature range. These observations corroborate that π–π interactions between the BODIPY dyes are hindered during the preorganization step, possibly induced in part by steric effects of the bulky trialkoxybenzene *meso*-substituents.

On the other hand, further cooling from 323 K to 283 K induces an overall signal broadening, which is more pronounced for the urea N–H protons and the aromatic protons from the benzene spacer than it is for the protons of the BODIPY core (Figure 4a). Particularly pronounced are the downfield shifts of N–H urea protons (H_j, cyan), which are by far the most affected resonances in VT- NMR (Figure 4a). This observation, in combination with the rise of a new broad carbonyl stretching band at 1700 cm^{-1} ($\Delta\nu = 24\ cm^{-1}$, Figure 4d) in FTIR, suggests the formation of intermolecular C=O···$(H–N)_2$ hydrogen bonds between the urea groups (323 K→283 K).

As a result of these interactions, an oligomerization process sets in, as evident from the overall broadening of all aromatic resonances in VT- NMR upon cooling to 283 K. To further analyze the packing of **1**, 2D ROESY investigations were performed at different stages of the self-assembly using different mixtures of $CDCl_3$ and MCH-d_{14}. In these studies, only the alkoxy chains exhibit new correlation signals (Figure S34), indicating their active involvement in shielding the oligomers from the aliphatic solvent, thereby contributing to restrict their extended growth. Apart from these interactions, no new correlation signals were detected compared to the monomer state in $CDCl_3$ (Figures 3 and S33,34), most likely indicating a parallel molecular arrangement to maximize the intermolecular H-bonding interactions between the urea units (C=O···$(H–N)_2$). This proposed packing is typically found in crystal structures of structurally related motifs,[49] and also supported by theoretical calculations. Due to the extended system size (268 atoms for a dimer), geometry optimization was performed by semi-empirical methods, as described in the Supporting Information. Two possible dimer conformations were optimized: a V-shaped dimer where the monomers are arranged in a parallel fashion (**D**) (Figure 4f) or a cross-shaped structure where the monomers are arranged orthogonally (**D1**) (Figure S39). While both types of packings have been previously observed for urea-based building blocks,[52] the parallel dimer is energetically more favorable ($< 7.89\ kJ\,mol^{-1}$) and supports the initial TD-DFT-optimized structure. In the optimized dimer **D**, bifurcated C=O···$(H–N)_2$ hydrogen bonds are observed with distances of 2.214 Å and 2.265 Å. Interestingly, a similar intramolecular C_{urea}=O···H_k–C hydrogen bond is observed in **D**, which further supports the optimized monomer using the TD-DFT approach. The hydrogen bonding distances are 2.082 Å, 2.089 Å (intramolecular), and 2.190 Å, 2.191 Å (intermolecular) (Figure 4f). This suggests that the initial monomer conformation may be maintained, at least in part, in the final assembly of **1**. To further investigate the potentially restricted rotation due to intramolecular C_{urea}=O···H_k–C hydrogen bonds, a similar calculation was performed for the dimeric model to obtain optimized structures **D2**, **D3** and **D4**. In this approach, the urea and the adjacent benzene rings were frozen while increasing the C_{urea}=O···H_k–C distances (Figure S39). Similar trends as for the monomer of **1** were observed: the overall stability of the dimer decreases upon increasing intramolecular hydrogen bond lengths.

To further elaborate on the origin of the anti-cooperative growth of **1** we expanded these calculations to short oligomers (trimer and tetramer) with methoxy groups (Figures S40, S41). The computations reveal nearly identical changes in Gibbs energy for each monomer addition, which would agree with an isodesmic growth. However, potential steric effects of the long dodecyloxy chains, which were not considered in the calculations to reduce computational costs, may also contribute to the observed weak anticooperative behaviour. Interestingly, we observe an increasingly less favorable addition for each monomer upon increasing the alkyl chain length, highlighting the influence of the alkyl chain flexibility (Figure S41 and Table S15).[34]

Morphological Analysis of the Self-Assembly

The size and shape of the assemblies formed by **1** were analyzed by combined atomic force microscopy (AFM), transmission electron microscopy (TEM), diffusion ordered spectroscopy (DOSY), small-angle X-ray scattering (SAXS) and dynamic light scattering (DLS). AFM studies, performed upon spin-coating aggregate solutions of **1** in MCH on highly-oriented pyrolytic graphite (HOPG), display small, distorted elliptical objects with a broad length (27.7 ± 8.1 nm) and width distribution (18.7 ± 7.8 nm) (see Figure 5b

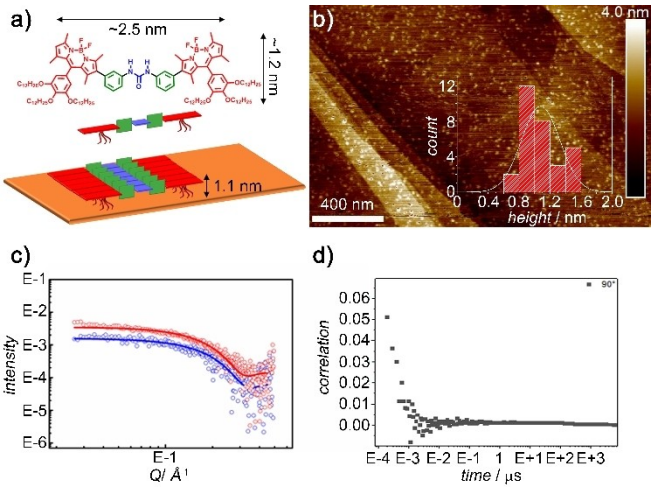

Figure 5. a) Cartoon representation of the molecular orientation of **1** on HOPG. b) AFM studies of **1** with corresponding height-profile histogram (inset). Solutions used for these studies: MCH at 20 µM and 273 K. c) Experimental SAXS profiles (circles) for **Agg1** in MCH at ≈2 mM (blue) and ≈4 mM (red) and the corresponding fittings (solid lines) to the customized model spheres. d) Correlation function of the DLS studies at 100 µM, 298 K in MCH.

and Table S5). Close analysis of 15 objects discloses an aspect ratio[53] of 1.6 ± 0.5 (isotropic systems exhibit an aspect ratio of 1), which is in agreement with the minor degree of anisotropy expected for an anti-cooperative growth.[35] Note that the extremely small size of the aggregates cannot be accurately determined by AFM owing to tip-sample convolution[54] leading to an artificial broadening.[55] Nevertheless, the observed length distributions are within the typical range of short oligomers.[22] Additionally, these small aggregates exhibit a uniform height of 1.1 ± 0.3 nm, which agrees well with the formation of 1D stacks of **1** that are arranged parallel to the HOPG substrate to maximize the interactions with the dodecyl chains (see Scheme in Figure 5a). These findings were further supported by TEM studies, which revealed nanoparticles with a similar size (Figure S35).

To further elucidate the size and morphology of the formed nanostructures in solution, combined DOSY, SAXS and DLS studies were performed (Figure 5 and Figure S36). DOSY experiments for molecularly dissolved **1** in $CHCl_3$ at 298 K and 1 mM unveil a hydrodynamic diameter of 2 nm, which matches the expected molecular length of ≈ 2.5 nm (Figure S36). Unfortunately, we were unable to obtain a sufficiently resolved DOSY signal in pure MCH under identical conditions due to the fast relaxation process in the aggregated state. Nevertheless, at slightly elevated temperatures (323 K) and weakened aggregation ($\alpha_{agg} \approx 0.9$), a hydrodynamic diameter of 2.2 nm was obtained. This value is only slightly larger than the monomer, and demonstrates that the formation of extended aggregates is unfavorable even at high concentration. The presence of discrete nanostructures, i.e. oligomers, not detectable in DLS experiments, is further supported by the rapid decay rates observed in the autocorrelation function (Figure 5d and S36).[56]

More accurate information on the size and morphology of the aggregates could be traced by SAXS experiments in MCH. Figure 5c shows the SAXS profiles for compound **1** at 2 and 4 mM. Both curves show practically no q^{-1} slope which is characteristic of non-fibrillar discrete aggregates. In this line, the experimental curves were found to fit best to the sphere customized model with a calculated radius of ≈ 13 Å (a diameter of ≈ 2.6 nm, see Supporting Information),[57] which remains invariant upon increasing concentration. These results indicate that the morphology of **Agg1** consists of spherical objects with an aspect ratio of close to 1,[35] in reasonable agreement with AFM. Remarkably, the radius obtained from the SAXS experiments matches well with the hydrodynamic diameter determined in DOSY and confirm the existence of small discrete aggregates that are typical for an anti-cooperative self-assembly process into short oligomers.

Conclusion

In conclusion, we have demonstrated a new tool to facilitate anti-cooperative self-assembly and maintained emission by combining a hydrogen bonding synthon with a sterically hindered appended dye moiety exhibiting pronounced conformational freedom. Thermodynamic analysis of the spectral changes observed in temperature- and concentration-dependent UV/Vis reveal that the newly designed BODIPY-appended urea-based chromophore **1** undergoes a weakly anti-cooperative self-assembly (**Agg1**). Detailed 1D and 2D NMR studies complemented with theoretical calculations demonstrate that the conformational freedom of **1** has a great impact on molecular preorganization and pre-nucleation events. The existence of intramolecular H-bonding between the urea carbonyl and the adjacent aromatic rings via C–H···O interactions preorganizes the molecular structure of **1** in an *anti–anti* conformation, which is effective for subsequent aggregate growth. However, increasing steric effects outweigh at some point intermolecular urea-urea H-bonding interactions, which limits the self-assembly to afford only small oligomers. The inability of **1** to form elongated polymers even at high concentrations has been demonstrated by DOSY NMR, DLS, SAXS, TEM and AFM, which are all consistent with the formation of small oligomers. Interestingly, due to the weak exciton coupling between the BODIPY dyes in the aggregate state, an efficient transfer of photophysical properties from the molecular to the supramolecular level is achieved. Remarkably, **Agg1** exhibits a fluorescence quantum yield in the range of molecularly dissolved **1** (26 % vs. 30 %) which is an uncommon phenomenon in the self-assembly of fluorescent dyes. Our results demonstrate the potential of combining hydrogen bonding with steric and conformational effects to control the size and photophysical properties of self-assembled structures. This approach might contribute to develop new functional materials based on self-assembled emissive dyes, with potential applications in the fields of biomedicine and imaging.

Acknowledgements

This work was supported in part by the National Science Foundation CHE-1904386 and OIA-1655740. I.H., N.B. and G.F. gratefully acknowledge the Deutsche Forschungsgemeinschaft (DFG) for funding (CRC 1450 inSight–431460824, IRTG 2678) for funding. B. S. thanks the MCIN/AEI/10.13039/501100011033, FSE "El FSE invierte en tu futuro" and FEDER "Una manera de hacer Europa" for the projects RYC-2017-21789 and EQC2018-004206-P. Open Access funding enabled and organized by Projekt DEAL.

Conflict of Interest

The authors declare no conflict of interest.

Data Availability Statement

The data that support the findings of this study are available in the Supporting Information of this article.

Keywords: Anti-Cooperativity · BODIPY Dyes · Conformational Changes · Self-Assembly · Hydrogen Bonding

[1] a) T. Aida, E. W. Meijer, *Isr. J. Chem.* **2020**, *60*, 33; b) A. W. Bosman, R. P. Sijbesma, E. W. Meijer, *Mater. Today* **2004**, *7*, 34; c) L. Brunsveld, B. J. Folmer, E. W. Meijer, R. P. Sijbesma, *Chem. Rev.* **2001**, *101*, 4071; d) L. Yang, X. Tan, Z. Wang, X. Zhang, *Chem. Rev.* **2015**, *115*, 7196.

[2] a) R. Dong, Y. Zhou, X. Huang, X. Zhu, Y. Lu, J. Shen, *Adv. Mater.* **2015**, *27*, 498; b) S. Cherumukkil, S. Ghosh, V. K. Praveen, A. Ajayaghosh, *Chem. Sci.* **2017**, *8*, 5644; c) G. Das, S. Cherumukkil, A. Padmakumar, V. B. Banakar, V. K. Praveen, A. Ajayaghosh, *Angew. Chem. Int. Ed.* **2021**, *60*, 7851; *Angew. Chem.* **2021**, *133*, 7930; d) V. K. Praveen, B. Vedhanarayanan, A. Mal, R. K. Mishra, A. Ajayaghosh, *Acc. Chem. Res.* **2020**, *53*, 496.

[3] T. Aida, E. W. Meijer, S. I. Stupp, *Science* **2012**, *335*, 813.

[4] C. Rest, R. Kandanelli, G. Fernández, *Chem. Soc. Rev.* **2015**, *44*, 2543.

[5] a) F. Würthner, *Acc. Chem. Res.* **2016**, *49*, 868; b) F. Würthner, C. R. Saha-Möller, B. Fimmel, S. Ogi, P. Leowanawat, D. Schmidt, *Chem. Rev.* **2016**, *116*, 962; c) Z. Chen, A. Lohr, C. R. Saha-Möller, F. Würthner, *Chem. Soc. Rev.* **2009**, *38*, 564.

[6] a) F. C. Spano, *Acc. Chem. Res.* **2010**, *43*, 429; b) T. Brixner, R. Hildner, J. Köhler, C. Lambert, F. Würthner, *Adv. Energy Mater.* **2017**, *7*, 1700236.

[7] N. J. Hestand, F. C. Spano, *Chem. Rev.* **2018**, *118*, 7069.

[8] a) S. Choi, J. Bouffard, Y. Kim, *Chem. Sci.* **2014**, *5*, 751; b) S. Kim, J. Bouffard, Y. Kim, *Chem. Eur. J.* **2015**, *21*, 17459.

[9] I. Helmers, N. Bäumer, G. Fernández, *Chem. Commun.* **2020**, *56*, 13808.

[10] I. Helmers, G. Ghosh, R. Q. Albuquerque, G. Fernández, *Angew. Chem. Int. Ed.* **2021**, *60*, 4368; *Angew. Chem.* **2021**, *133*, 4414.

[11] I. Helmers, M. Niehues, K. K. Kartha, B. J. Ravoo, G. Fernández, *Chem. Commun.* **2020**, *56*, 8944.

[12] F. Würthner, *Angew. Chem. Int. Ed.* **2020**, *59*, 14192; *Angew. Chem.* **2020**, *132*, 14296.

[13] J. Mei, N. L. C. Leung, R. T. K. Kwok, J. W. Y. Lam, B. Z. Tang, *Chem. Rev.* **2015**, *115*, 11718.

[14] a) F. Würthner, T. E. Kaiser, C. R. Saha-Möller, *Angew. Chem. Int. Ed.* **2011**, *50*, 3376; *Angew. Chem.* **2011**, *123*, 3436; b) P. B. Walczak, A. Eisfeld, J. S. Briggs, *J. Chem. Phys.* **2008**, *128*, 044505.

[15] I. Helmers, B. Shen, K. K. Kartha, R. Q. Albuquerque, M. Lee, G. Fernández, *Angew. Chem. Int. Ed.* **2020**, *59*, 5675; *Angew. Chem.* **2020**, *132*, 5724.

[16] a) Y. Hong, *Methods Appl. Fluoresc.* **2016**, *4*, 022003; b) Z. Zhao, H. Zhang, J. W. Y. Lam, B. Z. Tang, *Angew. Chem. Int. Ed.* **2020**, *59*, 9888; *Angew. Chem.* **2020**, *132*, 9972.

[17] a) G. Ghosh, P. Dey, S. Ghosh, *Chem. Commun.* **2020**, *56*, 6757; b) H. Kar, S. Ghosh, *Isr. J. Chem.* **2019**, *59*, 881; c) Y. Dorca, J. Matern, G. Fernández, L. Sánchez, *Isr. J. Chem.* **2019**, *59*, 869; d) S. Cherumukkil, B. Vedhanarayanan, G. Das, V. K. Praveen, A. Ajayaghosh, *Bull. Chem. Soc. Jpn.* **2018**, *91*, 100.

[18] S. Yagai, Y. Kitamoto, S. Datta, B. Adhikari, *Acc. Chem. Res.* **2019**, *52*, 1325.

[19] A. Sorrenti, J. Leira-Iglesias, A. J. Markvoort, T. F. A. de Greef, T. M. Hermans, *Chem. Soc. Rev.* **2017**, *46*, 5476.

[20] a) T. F. A. de Greef, M. M. J. Smulders, M. Wolffs, A. P. H. J. Schenning, R. P. Sijbesma, E. W. Meijer, *Chem. Rev.* **2009**, *109*, 5687; b) J. Matern, N. Bäumer, G. Fernández, *J. Am. Chem. Soc.* **2021**, *143*, 7164; c) J. J. van Gorp, J. A. J. M. Vekemans, E. W. Meijer, *J. Am. Chem. Soc.* **2002**, *124*, 14759; d) A. Suzuki, K. Aratsu, S. Datta, N. Shimizu, H. Takagi, R. Haruki, S.-I. Adachi, M. Hollamby, F. Silly, S. Yagai, *J. Am. Chem. Soc.* **2019**, *141*, 13196; e) D. González-Rodríguez, A. P. H. J. Schenning, *Chem. Mater.* **2011**, *23*, 310; f) Y. Kitamoto, Z. Pan, D. D. Prabhu, A. Isobe, T. Ohba, N. Shimizu, H. Takagi, R. Haruki, S.-I. Adachi, S. Yagai, *Nat. Commun.* **2019**, *10*, 4578; g) P. K. Hashim, J. Bergueiro, E. W. Meijer, T. Aida, *Prog. Polym. Sci.* **2020**, *105*, 101250; h) S. Cantekin, T. F. A. De Greef, A. R. A. Palmans, *Chem. Soc. Rev.* **2012**, *41*, 6125; i) S. Han, G. Mellot, S. Pensec, J. Rieger, F. Stoffelbach, E. Nicol, O. Colombani, J. Jestin, L. Bouteiller, *Macromolecules* **2020**, *53*, 427; j) A. Desmarchelier, B. G. Alvarenga, X. Caumes, L. Dubreucq, C. Troufflard, M. Tessier, N. Vanthuyne, J. Idé, T. Maistriaux, D. Beljonne, P. Brocorens, R. Lazzaroni, M. Raynal, L. Bouteiller, *Soft Matter* **2016**, *12*, 7824; k) X. Caumes, A. Baldi, G. Gontard, P. Brocorens, R. Lazzaroni, N. Vanthuyne, C. Troufflard, M. Raynal, L. Bouteiller, *Chem. Commun.* **2016**, *52*, 13369.

[21] M. F. Hagan, G. M. Grason, *Rev. Mod. Phys.* **2021**, *93*, 25008.

[22] Y. Vonhausen, A. Lohr, M. Stolte, F. Würthner, *Chem. Sci.* **2021**, *116*, 13279.

[23] a) F. Su, G. Chen, P. A. Korevaar, F. Pan, H. Liu, Z. Guo, A. P. H. J. Schenning, H.-J. Zhang, J. Lin, Y.-B. Jiang, *Angew. Chem. Int. Ed.* **2019**, *58*, 15273–15277; *Angew. Chem.* **2019**, *131*, 15417–15421; b) E. R. Zubarev, M. U. Pralle, L. Li, S. I. Stupp, *Science* **1999**, *283*, 523; c) V. Vázquez-González, M. J. Mayoral, R. Chamorro, M. M. R. M. Hendrix, I. K. Voets, D. González-Rodríguez, *J. Am. Chem. Soc.* **2019**, *141*, 16432; d) X. Li, L. E. Sinks, B. Rybtchinski, M. R. Wasielewski, *J. Am. Chem. Soc.* **2004**, *126*, 10810; e) R. Appel, J. Fuchs, S. M. Tyrrell, P. A. Korevaar, M. C. A. Stuart, I. K. Voets, M. Schönhoff, P. Besenius, *Chem. Eur. J.* **2015**, *21*, 19257.

[24] J. Gershberg, F. Fennel, T. H. Rehm, S. Lochbrunner, F. Würthner, *Chem. Sci.* **2016**, *7*, 1729.

[25] L. Herkert, J. Droste, K. K. Kartha, P. A. Korevaar, T. F. A. de Greef, M. R. Hansen, G. Fernández, *Angew. Chem. Int. Ed.* **2019**, *58*, 11344; *Angew. Chem.* **2019**, *131*, 11466.

[26] K. Cai, J. Xie, D. Zhang, W. Shi, Q. Yan, D. Zhao, *J. Am. Chem. Soc.* **2018**, *140*, 5764.

[27] a) N. Bäumer, J. Matern, G. Fernández, *Chem. Sci.* **2021**, *12*, 12248; b) P. Picchetti, G. Moreno-Alcántar, L. Talamini, A. Mourgout, A. Aliprandi, L. de Cola, *J. Am. Chem. Soc.* **2021**, *143*, 7681.

[28] a) K. Venkata Rao, D. Miyajima, A. Nihonyanagi, T. Aida, *Nat. Chem.* **2017**, *9*, 1133; b) P. A. Korevaar, C. Schaefer, T. F. A. de Greef, E. W. Meijer, *J. Am. Chem. Soc.* **2012**, *134*, 13482; c) G. M. Ter Huurne, P. Chidchob, A. Long, A. Martinez, A. R. A. Palmans, G. Vantomme, *Chem. Eur. J.* **2020**, *26*, 9964; d) E. Weyandt, L. Leanza, R. Capelli, G. M. Pavan, G. Vantomme, E. W. Meijer, *Nat. Commun.* **2022**, *13*, 248.

[29] R. van der Weegen, P. A. Korevaar, P. Voudouris, I. K. Voets, T. F. A. de Greef, J. A. J. M. Vekemans, E. W. Meijer, *Chem. Commun.* **2013**, *49*, 5532.

[30] R. Renner, M. Stolte, F. Würthner, *ChemistryOpen* **2020**, *9*, 32.

[31] D. Görl, X. Zhang, V. Stepanenko, F. Würthner, *Nat. Commun.* **2015**, *6*, 7009.

[32] P. P. N. Syamala, B. Soberats, D. Görl, S. Gekle, F. Würthner, *Chem. Sci.* **2019**, *10*, 9358.

[33] A. Arnaud, J. Belleney, F. Boué, L. Bouteiller, G. Carrot, V. Wintgens, *Angew. Chem. Int. Ed.* **2004**, *43*, 1718; *Angew. Chem.* **2004**, *116*, 1750.

[34] Y. Dorca, C. Naranjo, G. Ghosh, B. Soberats, J. Calbo, E. Ortí, G. Fernández, L. Sánchez, *Chem. Sci.* **2022**, *13*, 81.

[35] P. Besenius, G. Portale, P. H. H. Bomans, H. M. Janssen, A. R. A. Palmans, E. W. Meijer, *Proc. Natl. Acad. Sci. USA* **2010**, *107*, 17888.

[36] a) A. Rödle, M. Lambov, C. Mück-Lichtenfeld, V. Stepanenko, G. Fernández, *Polymer* **2017**, *128*, 317; b) X. Zhang, N. Zhou, X. Zhu, X. He, *Polym. Chem.* **2021**, *12*, 5535.
[37] Y. Zhang, P. Liu, H. Pan, H. Dai, X.-K. Ren, Z. Chen, *Chem. Commun.* **2020**, *56*, 12069.
[38] Y. Zhang, S. Yuan, P. Liu, L. Jing, H. Pan, X.-K- Ren, Z. Chen, *Org. Chem. Front.* **2021**, *8*, 4078.
[39] K. Tani, C. Ito, Y. Hanawa, M. Uchida, K. Otaguro, H. Horiuchi, H. Hiratsuka, *J. Phys. Chem. B* **2008**, *112*, 836.
[40] M. Kasha, H. R. Rawls, M. Ashraf El-Bayoumi, *Pure Appl. Chem.* **1965**, *11*, 371.
[41] a) P. A. Korevaar, T. F. A. de Greef, E. W. Meijer, *Chem. Mater.* **2014**, *26*, 576; b) J. Matern, Y. Dorca, L. Sánchez, G. Fernández, *Angew. Chem. Int. Ed.* **2019**, *58*, 16730; *Angew. Chem.* **2019**, *131*, 16884.
[42] M. M. J. Smulders, M. M. L. Nieuwenhuizen, T. F. A. de Greef, P. van der Schoot, A. P. H. J. Schenning, E. W. Meijer, *Chem. Eur. J.* **2010**, *16*, 362.
[43] R. F. Goldstein, L. Stryer, *Biophys. J.* **1986**, *50*, 583.
[44] a) D. S. Philips, K. K. Kartha, A. T. Politi, T. Krüger, R. Q. Albuquerque, G. Fernández, *Angew. Chem. Int. Ed.* **2019**, *58*, 4732; *Angew. Chem.* **2019**, *131*, 4782; b) F. Orvay, J. Cerdá, C. Rotger, E. Ortí, J. Aragó, A. Costa, B. Soberats, *Small* **2021**, *17*, 2006133.
[45] J.-D. Chai, M. Head-Gordon, *Phys. Chem. Chem. Phys.* **2008**, *10*, 6615.
[46] R. Ditchfield, W. J. Hehre, J. A. Pople, *J. Chem. Phys.* **1971**, *54*, 724.
[47] a) A. Schlachter, A. Fleury, K. Tanner, A. Soldera, B. Habermeyer, R. Guilard, P. D. Harvey, *Molecules* **2021**, *26*, 1780; b) A. Y. Shagurin, S. D. Usoltsev, Y. S. Marfin, *Comput. Theor. Chem.* **2019**, *1164*, 112553; c) T. Xu, C. Yan, Y. Wu, C. Yuan, X. Shao, *Dyes Pigm.* **2019**, *168*, 235.
[48] M. Matsumura, A. Tanatani, I. Azumaya, H. Masu, D. Hashizume, H. Kagechika, A. Muranaka, M. Uchiyama, *Chem. Commun.* **2013**, *49*, 2290.
[49] C. Capacci-Daniel, S. Dehghan, V. M. Wurster, J. A. Basile, R. Hiremath, A. A. Sarjeant, J. A. Swift, *CrystEngComm* **2008**, *10*, 1875.
[50] T. Cierpicki, J. Otlewski, *J. Biomol. NMR* **2001**, *21*, 249.
[51] L. S. Reddy, S. Basavoju, V. R. Vangala, A. Nangia, *Cryst. Growth Des.* **2006**, *6*, 161.
[52] M. S. Hossain, A. J. Sindt, D. W. Goodlett, D. J. Shields, C. J. O'Connor, A. Antevska, S. G. Karakalos, M. D. Smith, S. Garashchuk, T. D. Do, A. D. Gudmundsdottir, L. S. Shimizu, *J. Phys. Chem. C* **2021**, *125*, 19991.
[53] N. Sasaki, J. Yuan, T. Fukui, M. Takeuchi, K. Sugiyasu, *Chem. Eur. J.* **2020**, *26*, 7840.
[54] F. Gołek, P. Mazur, Z. Ryszka, S. Zuber, *Appl. Surf. Sci.* **2014**, *304*, 11.
[55] D. J. Keller, F. S. Franke, *Surf. Sci.* **1993**, *294*, 409.
[56] a) J. Stetefeld, S. A. McKenna, T. R. Patel, *Biophys. Rev. Lett.* **2016**, *8*, 409; b) S. Bhattacharjee, *J. Controlled Release* **2016**, *235*, 337.
[57] https://www.sasview.org.

Manuscript received: January 9, 2022
Accepted manuscript online: February 3, 2022
Version of record online: March 2, 2022